Correlation Assessment of NDVI and Land use Dynamics with Water Resources for the Southern Margin of Mu Us Sandy Land, China

Menglong Zhao
Yellow River Engineering Consulting Co Ltd
Yu Wang
Yellow River Conservancy Committee: Yellow River Conservancy Commission
Siyuan Liu (liusiyuan22@126.com)
Xi'an University of Technology https://orcid.org/0000-0002-1092-4456
Ping-an Zhong
Hohai University
Hongzhen Liu
Yellow River Engineering Consulting Co Ltd
Rongrong Li
Yellow River Engineering Consulting Co Ltd

Research Article

Keywords: Mu Us Sandy Land, water scarcity, NDVI, land use, impulse response function

Posted Date: May 24th, 2021

DOI: https://doi.org/10.21203/rs.3.rs-483664/v1

Version of Record: A version of this preprint was published at Environmental Science and Pollution Research on October 16th, 2021. See the published version at https://doi.org/10.1007/s11356-021-16757-3.

Correlation assessment of NDVI and land use dynamics with water resources for the southern margin of Mu Us Sandy Land, China

Menglong Zhao[a,b], Yu Wang[c], Siyuan Liu[d,*], Ping-an Zhong[b], Hongzhen Liu[e], Rongrong Li[e]

[a] *Yellow River Engineering Consulting Co.,Ltd.;Postdoctoral Research Station of Yellow River Engineering Consulting Co.,Ltd., Zhengzhou, Henan 450003, China*

[b] *College of Hydrology and Water Resources, Hohai University, NO.1, Xikang Road, Nanjing 210098, China*

[c] *Yellow River Conservancy Commission of the Ministry of Water Resources, Zhengzhou, Henan 450003, China*

[d] *State Key Laboratory of Eco-hydraulics in Northwest Arid Region, Xi'an University of Technology, Xi'an 710048, China*

[e] *Yellow River Engineering Consulting Co.,Ltd., Zhengzhou, Henan 450003, China.*

**Corresponding email: liusiyuan22@126.com*

Abstract: To prevent desertification, countries all over the world have made diversified efforts and vegetation restoration has been proved to be an effective approach. However, for sandy land that has limited water resources, measures such as artificial vegetation, may lead to the increase risk of drought. While affirming the achievements of sand utilization, there are many controversies exist regarding the advantages of turning deserts green, especially considering the water scarcity. Therefore, the long-run and causal relationships between sandy land, water consumption and vegetation coverage are necessary for explorations. Taken the southern margin of the Mu Us Sandy Land as the study area, this study explored the interactions between sandy land, water consumption and NDVI over a period of 2000-2018 with a VAR model approach. In the study area, various revegetation projects have made great achievements, resulting in a significant reduction of the sandy land area. In addition, the NDVI has ascend from 0.196 in 2000 to 0.371 in 2018 with a ratio of 89.3%. Results showed that there exist long-term stable equilibrium and causal relationships between water consumption with sandy land and NDVI. The increase of NDVI is relatively the direct factor causes the increase of water consumption. It could be inferred that those artificial vegetation measures may be based on large amount of water consumption,

which may aggravate further water shortage and ecological damage. More scientific and stronger water resources management measures need to be implemented locally to achieve a balance between water resources and revegetation.

Keywords: Mu Us Sandy Land; water scarcity; NDVI; land use; impulse response function

1 Introduction

Desertification is one of the most serious ecological problems worldwide. Drylands cover approximately 41% of Earth's land surface and are home to more than 38%of the total global population of 6.5 billion (James et al. 2007). To cope with the issue of desertification, governments around the world have implemented various measures, such as sand fixing, revegetation (Amiraslani and Dragovich 2011), installing windbreaks, and natural sealing (Zhu et al. 1984; Bonkoungou 1996). China, which is one of the most seriously affected countries by desertification, has been implementing large-scale conservation programs, including the Key Shelterbelt Construction Program, Wildlife Conservation and Nature Reserve Development Program, Forest Eco-Compensation Program, and Natural Forest Conservation Program (Liu et al. 2008; Yin and Yin 2010). The implementation of these projects has achieved remarkable results. According to the satellite data of NASA, the global green area increased by 5% from 2000 to 2017 (equivalent to the entire Amazon rainforest). Notably, China has been leading the growth of global greening and contributes 25% of the net growth in the global vegetation area (Chen et al. 2019).

The Mu Us Sandy Land, which is located in the typical agro-pastoral transitional zone, is one of the most sensitive, vulnerable and severely degraded areas in northern China. This desert area had rich water resources and high grass coverage; however, with an increase in population and human activities,

52 excessive reclamation and grazing led to water resource depletion and continuous desertification
53 (Runnström 2003; Huang et al. 2009; Bai and Cui 2019). However, in recent years, the trend of
54 desertification has reversed. The desertification land area of Mu Us Sandy Land reduced at an average
55 rate of 62.37 km^2/year from 1990 to 2017 (the desertification area in 2017 was 1684.09km^2) (Han et al.
56 2019). Over the past three decades, the interannual normalized difference vegetation index (NDVI) in
57 the Mu Us Desert mostly exhibited increasing trends due to human activity impacts (Karnieli et al. 2014;
58 Wu et al. 2014; An et al. 2014; Li et al. 2016). The area with the most dynamic NDVI trends is distributed
59 in the Shaanxi Province (Wu et al. 2002; Liu et al. 2020). This area occupies one-third of the area of Mu
60 Us Sandy Land and is known as the Agro-pastoral ecotone of the Northern Shaanxi Province (ANS).
61 According to data released by the Shaanxi Provincial Forestry Bureau on April 22, 2020 (Yulin Municipal
62 People's Government 2020), the desertification land control rate in Yulin has reached 93.24%, which
63 indicates that all mobile sand dunes have been fixed, which is the kind of real realization of "sand
64 degradation and green increase".

65 Due to the distinctiveness of the study location and the achievements of desertification prevention in
66 recent years, the ANS has become a research hotspot for scholars. Numerous studies have explored the
67 effectiveness of the aforementioned projects. Studies have explored the causes of desertification (Wu and
68 Ci 1999; Wu 2001), conducted monitoring and evaluation of desertification (Wu and Ci 2002; Zhang et
69 al. 2003), examined land use and land cover (LULC) changes (Zhang et al. 2012; Meng et al. 2012; Li
70 et al. 2013), explored the trends of vegetation change (Ju et al. 2008; Karnieli et al. 2014), and conducted
71 ecological risk and ecological vulnerability assessment in desert areas (Meng et al. 2015). However, the
72 transformation of a natural desert ecosystem is a complex coupling process and whether it will be the
73 causes of other changes is worth further exploration.

Previous studies have shown that both field investigation and statistical data analysis warned us that, by the common influence of the growing human activities and still fragile eco-environment, the ecological restoration in Mu Us are experiencing increasing challenges due to the water scarcity (Li et al. 2017).A previous study indicated that although revegetation has had positive effects on ecological systems in Mu Us Sandy Land, it has caused evapotranspiration to increase by 51 mm per summer; thus, revegetation has exacerbated water shortage in the aforementioned region (Zheng et al. 2020). In water-limited arid areas, a reduction in water resources due to vegetation results in a reduction in the amount of water available for human activities. Consequently, the competition for water between the environment and humans is exacerbated, which results in ecological degradation (Quiggin 2001; Wu et al. 2002). Field investigations and statistical data analyses have indicated that water-scarcity-related challenges are associated with the ecological restoration of the Mu Us Desert due to growing human activities and the fragile eco-environment in this region (Li et al. 2016, 2017). For sandy land that has limited water resources and is prone to a high degree of drought, measures, such as artificial vegetation, may lead to the increase of water consumption and then a new crisis of desertification. While affirming the achievements of sand utilization, there are many controversies exist regarding the advantages of turning deserts green, especially considering the scarcity of water resources in these areas. Therefore, will the degradation of sandy land lead to a substantial increase in water resources consumption and vegetation growth is necessary for consideration.

To address this issue, this study takes the ANS as the study area and aims (1) to analyze the change of land use in the study area and clarify the conversion relationship between sandy land and other land types, (2) to explore NDVI changes in the ANS, and (3) to access the dynamic relationships among sandy land, water resources, and the NDVI by using the vector autoregression (VAR) model. This study is expected

to provide references for the ecological improvement and sustainable development in water-deficient area.

2 Study area and data

2.1 Description of the study area

In this study, the Agro-pastoral ecotone of the Northern Shaanxi Province (ANS) is taken as the study area, which occupies one-third of the area of Mu Us Sandy Land. The ANS is located in northwest China (ranging from 107°35’ to 111°29’E and from 37°35’ to 39°02’N) and has an approximate area of 33 992 km^2 (Figure 1). It consists of six counties, namely Yuyang, Shenmu, Fugu, Hengshan, Dingbian, and Jingbian. More than 44.2% of the study area is classified as desertified land. The considered region has a typical continental semiarid climate and water resources here are very poor. The per capita water resources are only 9.97 million m^3, which is lower than the standard of water resources proposed by the United Nations Population Action Organization in 1993 for severely water-scarce countries (10 million m^3/per capita) (Wu and Ci 2002). The annual precipitation ranges from 440 mm in the southeast to 250 mm in the northwest. A total of 60%–80% of the annual precipitation is received from June to August. The annual mean temperature is approximately 6°C–8.5°C, with monthly mean temperatures of 22°C in July and −11°C in January.

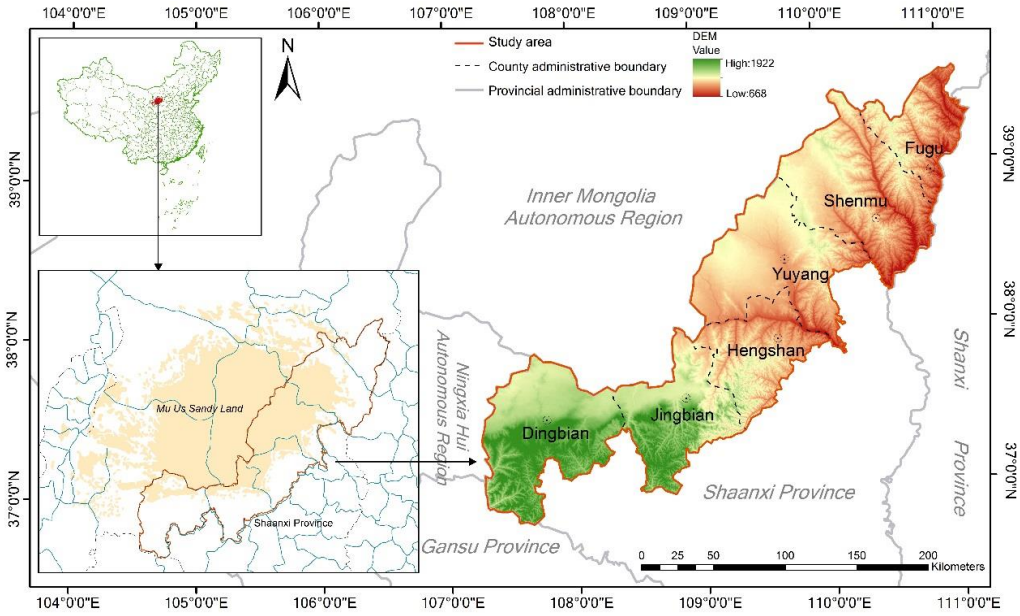

Fig.1 Location of the study area

2.2 Data sources

The types of land use represent the achievements of human beings in land use and transformation as well as the forms and uses (functions) of land. In this study, land use data from 1990 and 2000–2018 were used. These data were obtained from the remote sensing monitoring dataset of multiperiod LULC in China (CNLUCC). An efficient classification system was developed, and a research team from the Institute of Geographic Sciences and Natural Resources Research, Chinese Academy of Sciences, was invited to classify remote sensing image data through a human–machine interactive interpretation to achieve consistent and accurate classification (Liu et al. 2010). The NDVI is a quantitative parameter of vegetation coverage and reflects ecological environmental quality. Monthly average NDVI data were calculated from the spatial distribution dataset of China's monthly NDVI (2000–2018). The land use and NDVI data were obtained from the Resource and Environment Data Cloud Platform, Chinese Academy of Sciences (http://www.resdc.cn/).

Water resource data for 2000–2018 were mainly collected from the Water Resources Bulletin of Shaanxi Province and Water Resources Statistics Bulletin of Yulin City, which are available on the

websites of relevant government departments (http://slt.shaanxi.gov.cn/TJf-zxfw-Pb8-1-b9u-175 and http://slj.yl.gov.cn/index.html, respectively)

3 Methodology

3.1 Analysis of land use and NDVI changes

In order to better understanding the land cover change and NDVI trends in ANS, the evolution characteristics of land cover change and NDVI change were carried out. With ArcGIS platform, the land cover maps and NDVI change maps of 2000-2018 were overlaid, then key information on where experienced significant NDVI changes and what is the land cover type of this polygon were extracted.

Additionally, transition matrix, a classic method for detecting LUCC, has been employed for exploring dynamics of LUCC in ANS. For land cover changes of 2000-2018, the data were divided into four pairs of 2000-2005, 2005-2010, 2010-2015 and 2015-2018. For better comparison, the comparison between 1990 and 2000 has been supplemented. For each pair of compared data sets, an extended transition matrix was constructed. The maps from the initial and subsequent time were overlaid with ArcGIS to produce a matrix that provided the LULC areas by categorical transition between the two points in time. Due to the large amount of data, in order to better show the flow direction of data, Sankey chart was selected to show the data of transfer matrix.

3.2 A VAR model approach

The VAR model is a widely used econometrics technique for multivariate time-series modeling and proposed by Sims (1980) to analyze the mutual influence relationship between macroeconomic variables. VAR model has some very attractive features and has proven to be a valuable tool for analyzing dynamic transmission mechanisms among time-series processes (McMillan 1991; Lu 2001). In each equation of the model, endogenous variables return all lagged endogenous variable items to estimate dynamic

150 relationships among all the endogenous variables. Although the VAR model was originally developed
151 for analyzing the mutual influence relationship between macroeconomic variables, it uses simultaneous
152 multi-equations, which are not based on economic theory and can be applied to several other fields. For
153 example, the VAR model was used to analyze and forecast the mutual relationship between variables in
154 a system, determine leading and potential factors, and quantify the influence of these factors (Kumar et
155 al. 2009; Adenomon et al. 2013; Wu et al. 2018).

156 In addition to forecasting, VAR model equations are used to simulate the effects of sudden changes
157 (impulses) in one variable on other variables. Such effects are quantified through impulse response
158 function (IRF), which enable the estimation of the timescale over which changes in the water
159 consumption, sandy land area, and NDVI affect each other. Another application of the VAR model is the
160 variance decomposition with forecast error variance. The variance decomposition indicates what
161 percentage of a forecast error variance can be attributed to each individual variable used in the model.
162 The implementation of the VAR model is described in the following text.

163 *3.2.1 Augmented Dickey–Fuller test*

164 Standard Granger causality tests be conducted on stationary time series. The unit roots of X_t are
165 determined to confirm the stationary properties of each variable. The aforementioned unit roots are
166 obtained using the augmented Dickey–Fuller (ADF) test (Dickey and Fuller 1979, 1981). For the time
167 series X_t, the ADF relationship is expressed as follows:

168 $$\Delta X_t = \mu + \alpha X_{t-1} + \sum_{i=1}^{k} \beta_i \Delta X_{t-i} + \varepsilon_t \quad (1)$$

169 where Δ is the difference operator; k is the autoregressive lag length, that has to be sufficiently large
170 to eliminate possible serial correlation in β_i; α and β are the coefficients of interest. When the

aforementioned variables are found to be nonstationary, ADF tests are repeated for the first and second differences.

3.2.2 Johansen multivariate cointegration test

The Johansen multivariate cointegration test (Johansen and Juselius 1990) can be represented as follows:

$$\Delta Z_t = \mu + \prod Z_{t-1} + \sum_{i=1}^{k} \Gamma_i \Delta X_{t-i} + \varepsilon_t \quad (2)$$

where Z_t is a 3 × 1 vector of the variables $\ln U_t$, $\ln Y_t$, and $\ln E_t$; μ is a 3 × 1 vector of constant terms; Γ and Π represent 3 × 3 matrices of coefficients; and ε_t is a 3 × 1 vector of white noise error terms. The Johansen multivariate cointegration test is based on the maximum likelihood estimation and trace statistics (λ_{trace}), where λ_{trace} statistic tests the null hypothesis of no cointegration (rank(r) = 0) against an alternative hypothesis of cointegration (r > 0).

3.2.3 Selection of the lag length

Most VAR models are estimated using symmetric lags, that is, the same lag length is used for all variables in all equations of the model. The lag length is mostly selected using criteria such as the final prediction error (FPE) and Akaike information criterion (AIC). These information criteria are statistical model fit measures (Gao 2006). They quantify the relative goodness of fit of various previously derived statistical models for a given sample of data.

3.2.4 Impulse response function (IRF)

Because the VAR model is a nontheoretically model, directly determining the relationship among the variables in the model from parameter matrices is difficult. The aforementioned relationships can be obtained by analyzing the dynamic effect on the system when an error term changes or when the model

is shocked. Therefore, IRFs have been proposed as tools for interpreting VAR models. The impulse technique of response analysis involves representing the reaction of each variable to a shock in each equation of the system. IRFs can be used to reflect the effect of a random distribution term on the current and future values of endogenous variables. Thus, the dynamic effect of random disturbances on endogenous variables can be characterized. Such characterization reflects how a random disturbance influences other variables in accordance with the VAR model as well as the dynamic process of feedback to itself. IRFs with a strong time characteristic can indicate the degree of response for any new information generated by any system variable. A VAR can be modeled as a triangular moving average process, which can be written in the vector form as follows:

$$\frac{\partial x_{t+s}}{\partial \rho_{1t}} = \varphi_s \tag{3}$$

where the element of φ_s in row *i* and column *j* indicates the effect of a one-unit increase in the jth variable's innovation at time $t\left(\varepsilon_{ij}\right)$ on the value of the ith variable at time $t+s\left(x_{i,t+s}\right)$ when considering all other innovations at all times constant. Bootstrapped confidence intervals are commonly drawn around IRFs.

3.2.5 Variance decomposition

The variance decomposition is used to examine short-run dynamic interactions between model variables. The variance decomposition is used to describe a relativity effect, and it indicates how much of a forecast error variance can be attributed to each impact factor in the VAR system. Therefore, it is necessary to analyze the variance decomposition to trace the shocks to the system. The variance decomposition provides information regarding the relative importance of each random innovation in affecting the variables in the VAR model.

4 Results and discussion

4.1 Identifying the dynamic evolution in land use

As the rapid utilization of sand land in the ANS mainly began after 2000, LULC data for 1990 were selected here for compared with those for 2000–2018 to compare land use situations before and after sandy land utilization. As displayed in Figure 2, in 1990, the main land use categories in the ANS were cultivated land, grassland, and sandy land. The other land types occupied a limited area. The area of sandy land has decreased significantly since 1990, and sandy land has been gradually occupied by arable land and grassland. This trend remains the same after 2000. Moreover, the area of urban and rural construction land has increased rapidly, especially after 2000, which indicates that human activities have increased significantly in the study area. These human activities are concentrated in the marginal zone of sandy land distribution, which further proves that the scale of sand land utilization measures is gradually expanding.

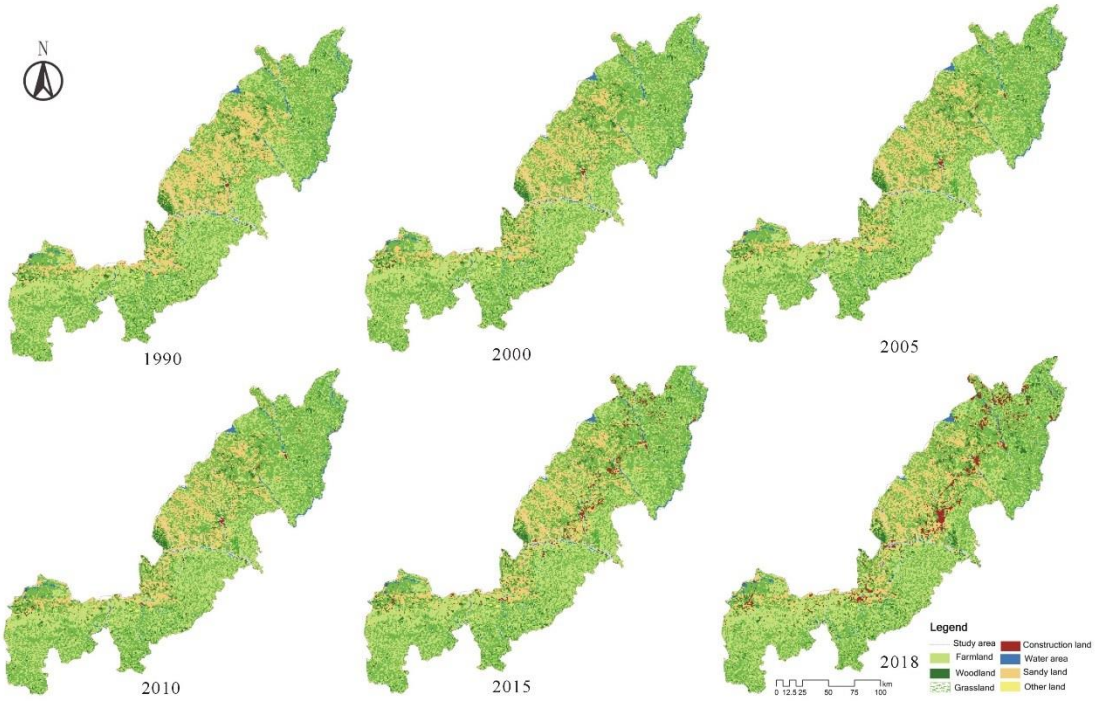

Fig.2 Land use maps of the study area from 1990 to 2018

227 The transition matrix, which is a classic tool for detecting LULC changes, was employed in this study
228 for exploring LULC changes in the ANS. An extended transition matrix was conducted for each pair of
229 compared datasets. The maps for the initial period and a subsequent period were overlaid to generate a
230 matrix that indicated the categorical transition in LULC over time (Pontius et al. 2004; Manandhar et al.
231 2010; Li et al. 2010). To better display data transfer in and out, the transfer matrix of land use was
232 obtained using ArcGIS software and visualized as a Sankey diagram (Figure 3) with data flow direction.
233 The Sankey diagram, which is also known as the Sankey energy balance diagram, is a specific type of
234 flow chart in which the width of the extended branch corresponds to the size of data flow. This diagram
235 was divided into five periods from 1990 to 2018. Figure 3 indicates that different types of land use in
236 each period were transferred out and in. The highest frequency of data conversion was obtained for the
237 period 2015–2018, followed by 1990–2000.
238 It is worth noting that the most frequent conversion between various types of land use occurred during
239 2015–2018 (mainly grassland, farmland, and sand). However, a certain balance existed between the
240 transfer in and transfer out, and the final change proportion was not significant. The final change
241 proportions for grassland, farmland, and sand were 1.3%, −2.7%, and −8%, respectively. Of all land
242 types, only the area of sandy land decreased continually. Since 1990, the sand area in the ANS decreased
243 from 5909.2 to 4114.8 km^2, with a total decrease of 30.4%. The main transferred-out type of sandy land
244 was grassland before 2010 and farmland after 2010. Moreover, construction land exhibited the highest
245 increase in area, from 89.5 km^2 in 1990 to 1016.4 km^2 in 2018 (11.4 times increase).
246 As above mentioned, the main transferred-out type of sandy land was grassland before 2010 and
247 farmland after 2010. In line with climatic conditions and rural living habits in the ANS, numerous
248 pastures and considerable cultivated land are distributed in this area. Irrespective of whether the sandy

land turned into grassland or farmland, the local agricultural water consumption and total water consumption was predicted to increase. To address this issue, it is necessary to explore the relationship of changes in the sandy land area with the total water consumption and agricultural water consumption.

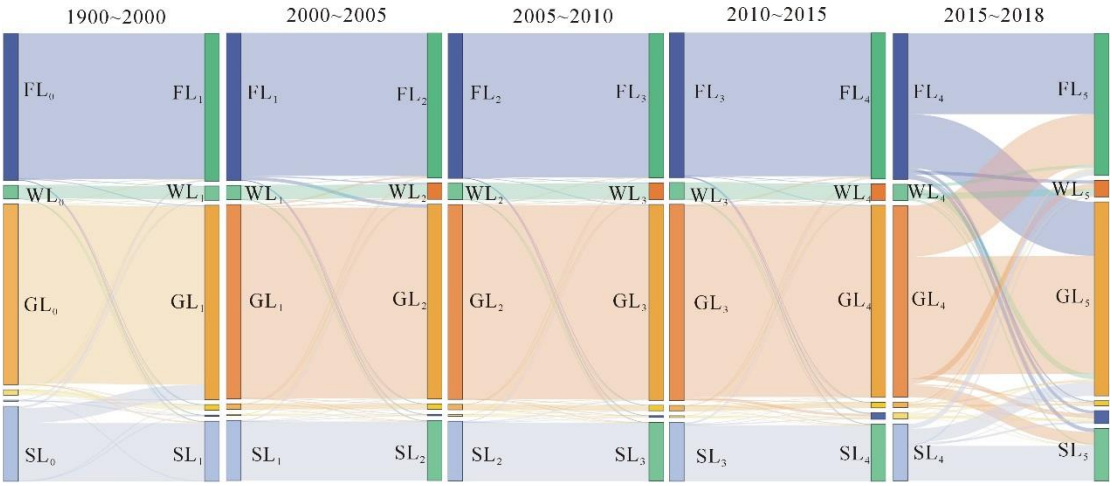

Note: FL denotes farmland, WL denotes woodland, GL denotes grassland, and SL denotes sandy land.

Fig.3 Sankey map of land use type conversion

4.2 Spatial and temporal evolution characteristics of the NDVI

Remote sensing data of the monthly average NDVI from 2000 to 2018 were obtained. The NDVI exhibited a fluctuating trend over 19 years but an increasing overall trend. The NDVI increased from 0.196 in 2000 to 0.371 in 2018. The total increase in the NDVI was 89.3%, with an average annual increase of 4.7%. After 2000, the highest obtained NDVI value was 0.594. This value was obtained in 2013. The annual maximum NDVI value was consistent with the overall trend of the annual average NDVI value. The annual maximum and annual average NDVI values exhibited growth trends. The annual average NDVI value exhibited a relatively stable growth, with a slope of 0.0092. The maximum NDVI value exhibited a higher volatility and more significant growth trend than the annual average NDVI value did. The slope of the trend of the maximum NDVI value was 0.0132. The average annual NDVI of the entire ecotone was 0.279.

In terms of NDVI distribution within year, the vegetation coverage increased significantly after May.

The vegetation coverage from May to October was significantly higher than that during other periods of the year. In addition, the average monthly NDVI reached a maximum value of 0.473 in August, which was consistent with the growth period of vegetation and crops in the ANS. Subsequently, the vegetation gradually withered and the NDVI began to decline. The lowest NDVI of 0.160 was observed in February.

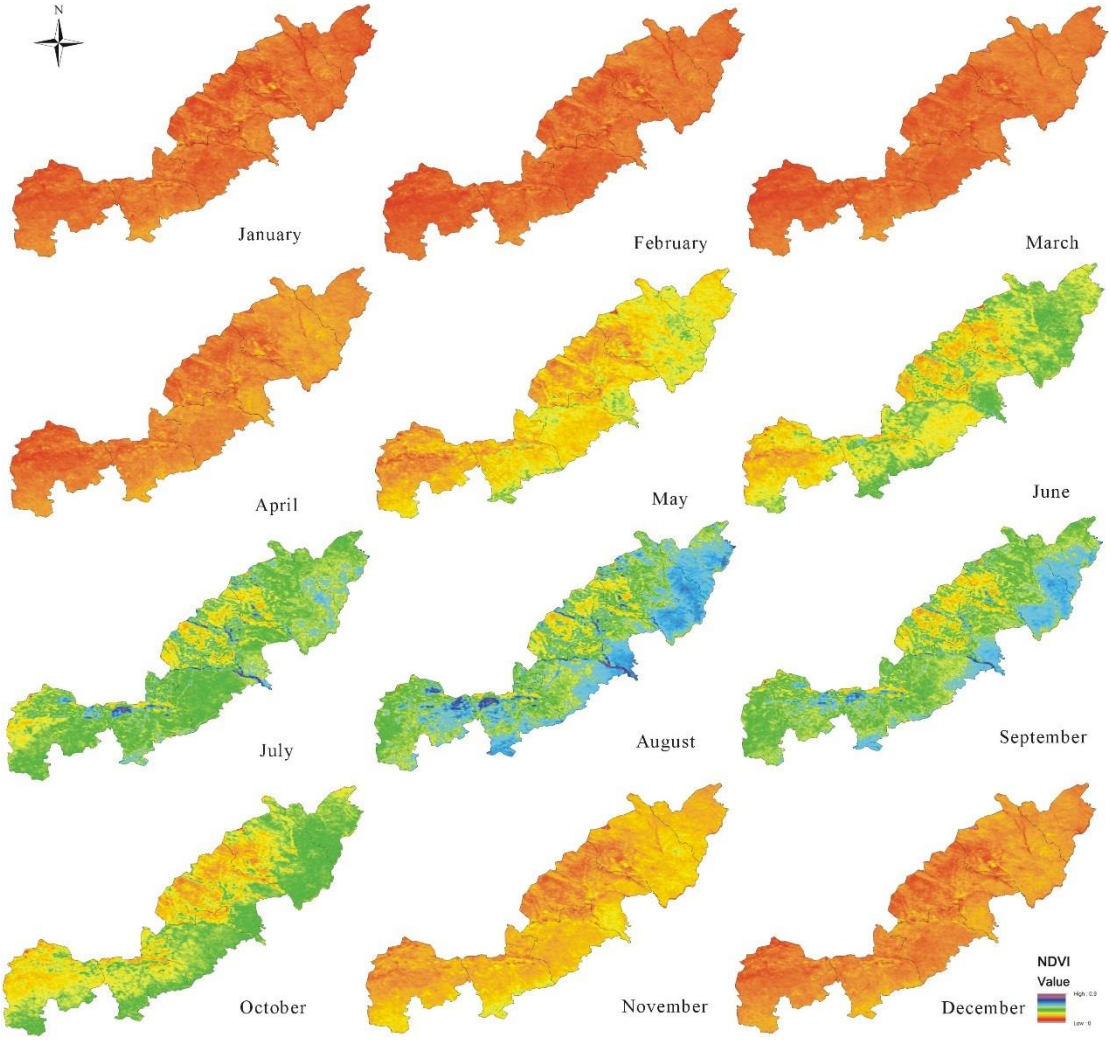

Fig.4 Distribution of the NDVI in the ANS within year

Due to differences in natural conditions and geographical characteristics, the vegetation coverage exhibited an uneven distribution in space and time (Figure 4). Regions with high NDVI values were concentrated in the southeast of the ANS. The vegetation coverage in the northwest was relatively low, which is consistent with the distribution of loess and desert from southeast to northwest; thus, the vegetation growth was poor in regions close to sand and water-deficient areas. Moreover, the NDVI in

278 the middle of the ANS was lower than that in other regions. Ultimately, the evolution of the NDVI
279 indicated that the vegetation coverage in the entire ecotone gradually improved, which is beneficial for
280 the ecological improvement of the ecotone.

281 **4.3 Dynamic relationships of sandy land, water consumption and NDVI**

282 *4.3.1 Analysis for stationarity and cointegration test*

283 The stationarity of standardized time series of the total water consumption (*TC*), agricultural water
284 consumption (*AC*), sandy area (*SA*), and NDVI (*NV*) of the study area was examined. To avoid data
285 fluctuation and eliminate possible heteroscedasticity, the data were first subjected to logarithm
286 processing. The obtained data sequence was then subjected to ADF testing. According to the results of
287 ADF test (Table 1), the data sequence was stable if the prob. value was less than 0.05 (95% confidence
288 interval) and the ADF statistic was less than the critical values of 1%, 5%, and 10% significance levels.
289 According to Table 1, all data sequences were nonstationary in the original sequence state. The prob.
290 values of *log(TC)*, *log(AC)*, and *log(NV)* were less than 0.05 after the first-order difference; thus, these
291 sequences reached a stable state. Only the *log(SA)* sequence reached a stable state after the second-order
292 difference. Considering that only the same order stationary may prevent pseudo regression, the second-
293 order difference was applied to all data sequences to obtain the stationary sequence.
294
295
296
297
298
299

Table 1 Stationarity test results for each variable

Sequence	ADF-Statistic	Prob. Value	Critical values at different significant level			Conclusion
			1%	5%	10%	
$\log(TC)$	-0.795659	0.79561	-3.857386	-3.040391	-2.660551	Unstable
$\nabla\log(TC)$	-4.686907	0.0001	-2.708094	-1.962813	-1.606129	Stable
$\nabla'\log(TC)$	-4.443680	0.0003	-2.754993	-1.970978	-1.603693	Stable
$\log(AC)$	-3.404071	0.0248	-3.857386	-3.040391	-2.660551	Unstable
$\nabla\log(AC)$	-6.951639	0.0000	-2.708094	-1.962813	-1.606129	Stable
$\nabla'\log(AC)$	-4.289001	0.0004	-2.754993	-1.970978	-1.603693	Stable
$\log(SA)$	4.801633	1.0000	-3.920350	-3.065585	-2.673459	Unstable
$\nabla\log(SA)$	1.480889	0.9582	-2.728252	-1.966270	-1.605026	Unstable
$\nabla'\log(SA)$	-5.601733	0.0000	-2.728252	-1.966270	-1.605026	Stable
$\log(NV)$	0.067579	0.9521	-3.920350	-3.065585	-2.673459	Unstable
$\nabla\log(NV)$	-3.405363	0.0020	-2.708094	-1.962813	-1.606129	Stable
$\nabla'\log(NV)$	-6.714835	0.0000	-2.728252	-1.966270	-1.605026	Stable

Note: ∇ refers to the first-order difference and ∇' refers to the second-order difference.

After the differential processing of time series to make them stable, data sequences may lack long-term information, which is essential for problem analysis. The cointegration test is used to test whether the causal relationship described by a regression equation is pseudo regression, that is, to test whether a stable relationship exists among variables. In Johansen cointegration test, the maximum likelihood estimation is used to analyze cointegration relationships among multiple variables.

As presented in Table 2, when the number of cointegration equations was 0, the trace statistics and maximum eigenvalue statistics were 107.8306 and 55.35650, respectively, which are greater than the critical value for a significance level of 5%. Therefore, the original hypothesis of "zero cointegration relationships" is rejected. The results of the trace statistics test and Max–Eigen statistics test indicated

311 that cointegration relationships, that is, long-term stable equilibrium relationships, existed among the
312 sequences. These relationships were not affected by short-term fluctuations.

313 **Table 2** Results of the Johansen multivariate cointegration test

Trace test				
H_0	Statistic	Trace Statistic	0.05 critical value	Proc. Value
None *	0.975093	107.8306	40.17493	0.0000
At most 1 *	0.855498	52.47411	24.27596	0.0000
At most 2 *	0.683380	23.45716	12.32090	0.0005
At most 3 *	0.338838	6.203644	4.129906	0.0151
Max-eigenvalue test				
H_0	Statistic	Max-Elgen Statistic	0.05 critical value	Proc. Value
None *	0.975039	55.35650	24.15921	0.0000
At most 1 *	0.855498	29.01696	17.79730	0.0007
At most 2 *	0.683380	17.25081	11.22480	0.0039
At most 3 *	0.338838	6.206344	4.129906	0.1051

314 Note: * indicates rejection of the original hypothesis at a significance level of 5%.

315 *4.3.2 Construction of VAR model*

316 An important aspect of the VAR model is the determination of a suitable lag length. If the lag length
317 is too short, the dynamic relationship between variables cannot be fully reflected. Moreover, if the lag
318 length is too long, the degree of freedom can decrease and the validity of the estimated model parameters
319 may be affected. Therefore, a balance must be found between the lag period and the degree of freedom.

320 Different information criteria, including the Final prediction error (FPE), Akaike information criterion
321 (AIC), Schwartz information criterion (SC), Hannan–Quinn (HQ) criterion, and likelihood ratio (LR)
322 test, were used to calculate the lag length for the VAR model. The test results (Table 3) indicate that the
323 maximum lag recommended by the information criteria is 2.

Table 3 Lag length selection for the VAR model

lag	LogL.	LR	FPE	AIC	SC	HQ
0	106.5353	NA	1.36e-11	-13.67137	-13.48256	-13.67339
1	124.5452	24.01314	1.15e-11	-13.93935	-12.99529	-13.94941
2	166.4638	33.53488*	6.90e-13*	-17.393517*	-15.69585*	-17.41327*

The VAR model equation for runoff obtained through the E-views software can be written as follows:

$$
\begin{cases}
\nabla LOG(TC) = -0.357571*\nabla LOG(TC)(-1) + 0.0428919*\nabla LOG(TC)(-2) \\
\quad -0.520934*\nabla LOG(AC)(-1) - 0.683777*\nabla LOG(AC)(-2) - 3.53318*\nabla LOG(SA)(-1) \\
\quad -2.68867*\nabla LOG(SA)(-2) + 0.246604*\nabla LOG(NV)(-1) - 0.174807*\nabla LOG(NV)(-2) - 0.0002380 \\
\nabla LOG(AC) = 0.150301*\nabla LOG(TC)(-1) - 0.0129580*\nabla LOG(TC)(-2) \\
\quad -1.35860*\nabla LOG(AC)(-1) - 0.826909*\nabla LOG(AC)(-2) - 3.21678*\nabla LOG(SA)(-1) \\
\quad -2.66472*\nabla LOG(SA)(-2) + 0.383647*\nabla LOG(NV)(-1) - 0.153425*\nabla LOG(NV)(-2) - 0.00398098 \\
\nabla LOG(SA) = -0.22980*\nabla LOG(TC)(-1) + 0.0928248*\nabla LOG(TC)(-2) + 0.233267*\nabla LOG(AC)(-1) \\
\quad +0.105044*\nabla LOG(AC)(-2) - 0.657593*SA(-1) - 0.222565*\nabla LOG(SA)(-2) \\
\quad -0.0078130*\nabla LOG(NV)(-1) - 0.0600037*\nabla LOG(NV)(-2) - 0.00291671 \\
\nabla LOG(NV) = 0.970659*\nabla LOG(TC)(-1) - 0.036026*\nabla LOG(TC)(-2) - 1.08938*\nabla LOG(AC)(-1) \\
\quad -0.53202*\nabla LOG(AC)(-2) - 1.85507*\nabla LOG(SA)(-1) - 2.07679*\nabla LOG(SA)(-2) \\
\quad -0.0997239*\nabla LOG(NV)(-1) - 0.30593*\nabla LOG(NV)(-2) - 0.0122083
\end{cases}
$$

4.3.3 Analysis of impulse response and relative contribution

The relationships among the variables were investigated by determining shocks in one variable and examining whether these shocks were transmitted to other variables. The aforementioned investigation was performed through impulse response analysis within the context of the VAR model.

Results in Figures 5 reveal that one of the four variables ($\nabla\log(TC)$, $\nabla\log(AC)$, $\nabla\log(SA)$, and $\nabla\log(NV)$) had a significant initial effect on the other variables. The initial effects of $\nabla\log(SA)$, and $\nabla\log(NV)$ on other variables were marginally stronger and longer than those of $\nabla\log(SA)$ and $\nabla\log(NV)$ on other variables (Figure 5). This result indicates that the relationships

335 of sand area and vegetation coverage with the water consumption were significant. With the reduction of
336 sandy land converted into vegetation cover, then the increase of vegetation coverage will be the direct
337 factor causes the increase of water consumption. The change of sandy land area is an indirect factor. The
338 results show that the response of water consumption to the change of NDVI is relatively stronger.

339 Furthermore, $\nabla\log(TC)$, $\nabla\log(AC)$, and $\nabla\log(SA)$ responded to a positive $\nabla\log(NV)$
340 shock begin with the horizontal line and after one step for each point of the sample. Similarly, the
341 responses of $\nabla\log(TC)$ and $\nabla\log(AC)$ to a negative $\nabla\log(SA)$ shock exhibited a lag of one
342 period. To some extent, water consumption and sand changes can be considered to respond to the
343 vegetation growth in the second year of growth. In other words, the vegetation has an impact on water
344 consumption and sand land after a certain period of growth and accumulation, which performed the
345 characteristic of lagging.

346 The responses of sandy land to other variables were very significant. No signs of decline were observed
347 over 10 periods, which proved that the responses of sandy land to other variables, especially water
348 consumption ($\nabla\log(TC)$ and $\nabla\log(AC)$), were sensitive and had long-term stability. The response
349 of $\nabla\log(SA)$ to $\nabla\log(NV)$ exhibited hysteresis loops and an increasing trend with time, which
350 may have a cumulative effect. Results indicate that the changes in the sandy land area may be negatively
351 affected by NDVI. Thus, the longer the NDVI continues to increase, the greater is its effect on the
352 transformations of the sandy land area.

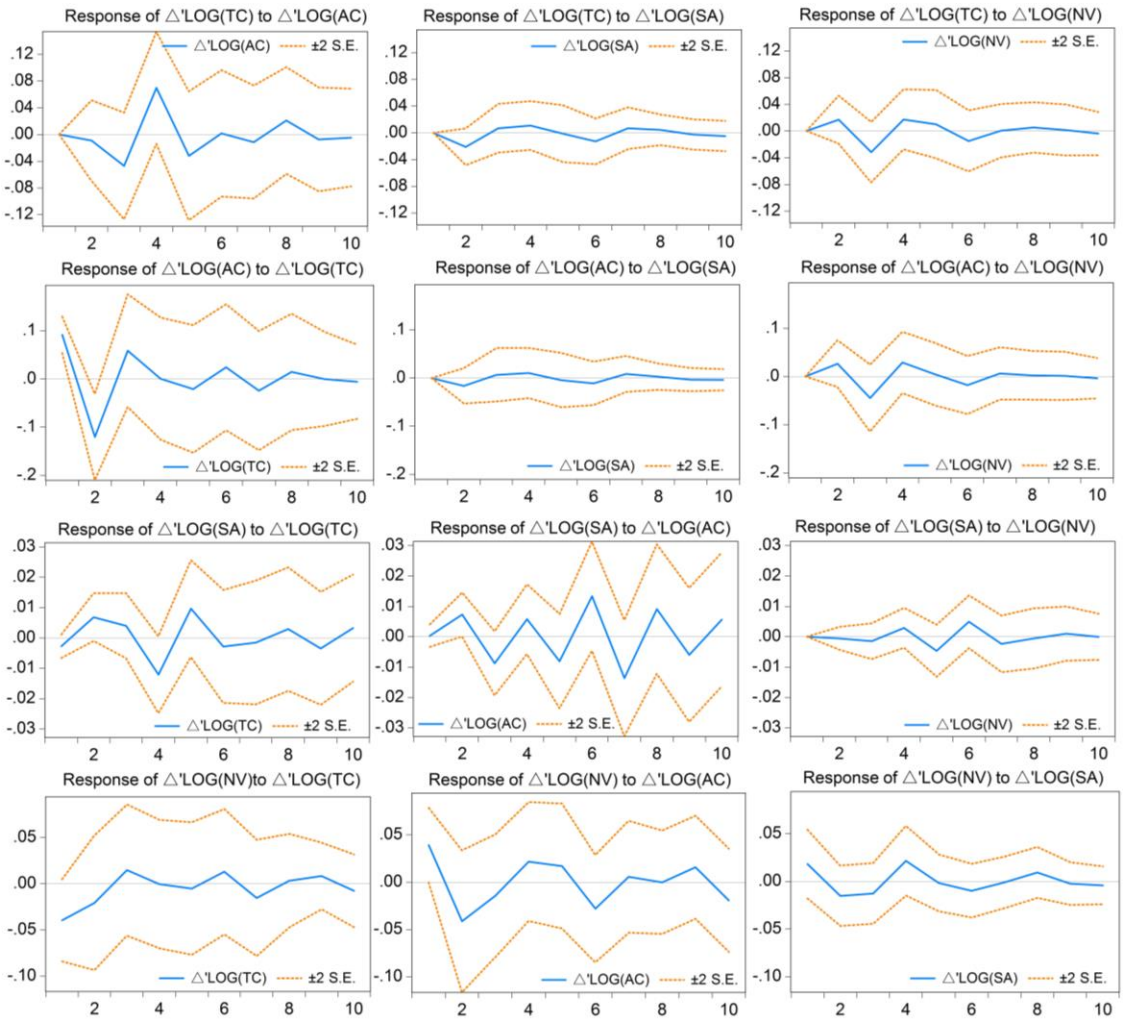

Fig.5 Impulse responses chart

The variance decomposition was employed identify the proportion of variance in one variable caused by the innovations in other variables in a vector autoregressive (VAR) system. The variance decomposition results obtained in this study are presented in Table 4. Relatively, NDVI has a strong impact on the total water consumption and agricultural water consumption, which are about 8% and 9% respectively, and show an increasing trend with time. This also confirms the results of IRF, that the growth of vegetation coverage has a direct effect on water consumption.

It should be noted that sandy land area and NDVI are closely related to agricultural water consumption, which are shown in Table 4 and gradually increase with time. It is believed that the process of sandy land transforming into other land use types will have a significant impact on agricultural water consumption.

In ANS, all the water consumption of farmland, woodland and grassland belongs to agricultural water. It can be concluded that the development and utilization measures of sand land in ANS area may be based on large amount of water consumption. Thus, the growth of vegetation is based on investment in water resources. This phenomenon may serve as a reminder that while various measures implemented for combating desertification, it should be alert to the increase of water consumption, which may cause further impact on water shortage areas. Therefore, the scientific management of water resources is an effective strategy for transforming sandy land and achieving vegetation growth. To achieve sustainable development of the local natural system, a balance must be realized among water resources, sandy land area, and vegetation coverage.

386 **Table 4** Variance decomposition results (%)

Variance Decomposition of $\nabla\log(TC)$					Variance Decomposition of AC			
Period	$\nabla\log(TC)$	$\nabla\log(AC)$	$\nabla\log(SA)$	$\nabla\log(NV)$	$\nabla\log(TC)$	$\nabla\log(AC)$	$\nabla\log(SA)$	$\nabla\log(NV)$
1	1	0	0	0	88.14	11.86	0.00	0.00
2	92.98	0.72	3.80	2.50	88.04	8.27	1.01	2.68
3	72.86	15.30	3.24	8.59	80.93	9.82	0.94	8.31
4	54.58	34.78	2.94	7.70	67.91	21.86	1.08	9.15
5	52.40	37.16	2.76	7.68	64.75	25.55	1.06	8.64
6	51.94	36.19	3.41	8.46	64.43	25.11	1.31	9.15
7	52.09	36.05	3.55	8.30	64.60	24.87	1.45	9.07
8	51.19	37.05	3.55	8.22	64.27	25.31	1.45	8.97
9	51.06	37.17	3.57	8.20	64.17	25.39	1.48	8.96
10	50.98	37.13	3.65	8.24	64.12	25.41	1.50	8.97
Variance Decomposition of $\nabla\log(SA)$					Variance Decomposition of $\nabla\log(NV)$			
Period	$\nabla\log(TC)$	$\nabla\log(AC)$	$\nabla\log(SA)$	$\nabla\log(NV)$	$\nabla\log(TC)$	$\nabla\log(AC)$	$\nabla\log(SA)$	$\nabla\log(NV)$
1	12.63	0.22	87.15	0. 00	19.07	1892	4.04	0.57.98
2	29.58	29.16	41.10	0.16	18.72	30.74	5.29	45.24
3	24.98	46.21	27.94	0.87	18.10	28.41	5.92	47.58
4	45.46	34.27	17.97	2.30	16.59	29.65	8.95	44.80
5	46.47	34.20	14.46	4.87	16.08	30.52	8.60	44.80
6	36.15	46.19	11.18	6.48	15.89	33.13	8.53	42.45
7	29.83	55.18	9.17	5.82	17.13	32.77	8.39	41.72
8	28.17	57.90	8.55	5.38	17.09	32.55	8.90	41.47
9	27.94	58.35	8.47	5.24	17.16	33.40	8.73	40.70
10	27.81	58.88	8.26	5.06	17.04	34.72	8.60	39.64

387 **5 Conclusions**

388 China has been leading the growth of global greening after 2000 and contributes 25% of the net growth

389 in the global vegetation area. To explore the reasons behind, is the desertification control measures and

vegetation enhancement project have made steady achievements. For sandy land that has limited water resources and is prone to a high degree of drought, measures, such as artificial vegetation, may lead to the increase of water consumption and then a new crisis of desertification. While affirming the achievements of sand utilization, there are many controversies exist regarding the advantages of turning deserts green, especially considering the scarcity of water resources in these areas. Therefore, the long-run and causal relationship between sandy land, water consumption and vegetation coverage are necessary for explorations.

The ANS, located in the southern margin of the Mu Us desert of China, was taken as the study area in this study. The interactions between sandy land, water consumption and NDVI over a period of 2000-2018 were examined with VAR model. The results indicate that:

(1) The implementation of desertification control projects makes the ANS experienced frequent land transformation and the sandy area decreased constantly. The main transferred-out type of sandy land was grassland before 2010 and farmland after 2010.

(2) With significant increase, the NDVI ascend from 0.196 in 2000 to 0.371 in 2018 with a ratio of 89.3%. However, its spatial distribution was uneven. Especially in the area along the sandy land distribution, the intensity of human disturbance is high, while the vegetation coverage is low. For further sand control measures, ecological vulnerability should be considered scientifically.

(3) There existed long-term stable equilibrium and causal relationships among water consumption, sandy land and NDVI. Relatively, NDVI has a strong impact on the water consumption and show an increasing trend with time. The increase of NDVI may be the direct factor causes the increase of water consumption, and the change of sandy land area is an indirect factor.

It could be concluded that the development and utilization measures of sand land in ANS area may be

based on large amount of water consumption. Thus, the growth of vegetation is based on investment in water resources. This phenomenon may serve as a reminder that while various measures implemented for combating desertification, it should be alert to the increase of water consumption, which may cause further impact on water shortage areas. Therefore, the scientific management of water resources is an effective strategy for transforming sandy land and achieving vegetation growth. To achieve sustainable development of the local natural system, a balance must be realized among water resources, sandy land area, and vegetation coverage.

Declarations：

Ethics approval and consent to participate： Not applicable.

Consent for publication: Not applicable.

Availability of data and materials: The datasets analyzed during the current study are available in the following data sets. Xu Xinliang. Spatial distribution data set of monthly vegetation index (NDVI) in China. Data registration and publishing system of resource and environmental science data center, Chinese Academy of Sciences（ http://www.resdc.cn/DOI),2018.DOI:10.12078/2018060602

Competing interests: The authors declare that they have no competing interests.

Funding: This study was supported by the Postdoctoral research and development project of Yellow River Engineering Consulting Co.,Ltd. (Grant No.2020BSHZL04), and the National Key Research and Development Program of China (Grant No. 2017YFC0404402, 2018YFC1508404).

Authors' contributions: MZ and YW designed the concept and methodology developed in this article and selected the case study, together with the other co-authors; SL prepared the initial draft manuscript and analyzed the results under supervision of YW and PZ.; HL and RL made the final editing and revision

work. All authors read and approved the manuscript to submission.

References

Adenomon, M. O., Ojehomon, V. E., Oyejola, B. A. (2013) Modelling The Dynamic Relationship Between Rainfall and Temperature Time Series Data In Niger State, Nigeria. Mathematical theory and modeling 3(4):53-70. https://doi.org/10.7176/MTM

Amiraslani, F., & Dragovich, D. (2011) Combating desertification in Iran over the last 50 years: an overview of changing approaches. Journal of Environmental Management 92(1):1-13. DOI: 10.1016/j.jenvman.2010.08.012

An, Y., Gao, W., & Gao, Z. (2014). Characterizing land condition variability in Northern China from 1982 to 2011. Environmental Earth Sciences 72(3):663-676. DOI:10.1007/s12665-013-2987-6

Bai Z., Cui J. (2019). Desertification and its causes in Mu Us Desert in recent 2000 years, 39(2): 177-185. DOI: 10.7522/j.issn.1000-694X.2019.00007

Bonkoungou E G. (1996) Drought, desertification, and water management in sub-Saharan Africa. United Nations University Press, New York, NY, E.-U, 165-180.

Chen, C., Park, T., Wang, X. et al. (2019) China and India lead in greening of the world through land-use management. Nature Sustainability 2.2: 122-129. https://doi.org/10.1038/s41893-019-0220-7

Dickey, D. A., & Fuller, W. A. (1979) Distribution of the Estimators for Autoregressive Time Series with a Unit Root. Journal of the American Statistical Association, 74(366):427-431. https://doi.org/10.1080/01621459.1979.10482531

Dickey, D. A., & Fuller, W. A. (1981). Likelihood Ratio Statistics for Autoregressive Time Series with a Unit Root. Econometrica, 49(4), 1057-1072. https://doi.org/10.2307/1912517

456 Engle, R. F., & Granger, C. W. (1987 Co-integration and Error Correction: Representation, Estimation,
457 and Testing. Econometrica, 55(2):251-276. https://doi.org/10.2307/1913236
458 Gao, T. M. (2006). Econometric analysis and modeling—EVIEWS examples and cases. Beijing,
459 Tsinghua University Press
460 Huang, Y., Wang, N., He, T., Chen, H., Zhao, L. (2009). Historical desertification of the Mu Us Desert,
461 Northern China: A multidisciplinary study. Geomorphology, 110(3), 108-117.
462 https://doi.org/10.1016/j.geomorph.2009.03.020
463 Jiyuan, L., Zengxiang, Z., Xinliang, X., Wenhui, K., Wancun, Z., Shuwen, Z., et al. (2010) Spatial
464 patterns and driving forces of land use change in China during the early 21st century. Journal of
465 Geographical Sciences, 20(4):483-494. DOI:10.1007/s11442-010-0483-4
466 Johansen, S., & Juselius, K. (1990) Maximum likelihood estimation and inference on cointegration with
467 application to the demand for money. Oxford Bulletin of Economics and Statistics, 52:169-210.
468 DOI:10.1111/j.1468-0084.1990.mp52002003.x
469 Ju, C., Cai, T., & Yang, X. (2008) Topography-based modeling to estimate percent vegetation cover in
470 semi-arid Mu Us sandy land, China. Computers and Electronics in Agriculture, 64(2):133-139.
471 DOI:10.1016/j.compag.2008.04.008
472 Karnieli, A., Qin, Z.H., Wu, B., Panov, N., Yan, F. (2014) Spatio-temporal dynamics of land-use and
473 land-coverin the Mu Us Sandy Land, China, using the change vector analysis technique. Remote
474 Sensing. 6 (10), 9316–9339. DOI:10.3390/rs6109316
475 Kumar, U., Prakash, A., & Jain, V. K. (2009) A Multivariate Time Series Approach to Study the
476 Interdependence among O3, NOx, and VOCs in Ambient Urban Atmosphere. Environmental
477 Modeling & Assessment, 14(5):631-643. DOI:10.1007/s10666-008-9167-1

478 Li, J., Zhao, Y., Liu, H., & Su, Z. (2016) Sandy desertification cycles in the southwestern Mu Us Desert
479 in China over the past 80 years recorded based on nebkha sediments. Aeolian Research, 100-107.
480 DOI:10.1016/j.aeolia.2015.12.003
481 Li, Y., Cao, Z., Long, H., Liu, Y., & Li, W. (2017) Dynamic analysis of ecological environment combined
482 with land cover and NDVI changes and implications for sustainable urban–rural development: The
483 case of Mu Us Sandy Land, China. Journal of Cleaner Production, 142(PT.2):697-715.
484 DOI:10.1016/j.jclepro.2016.09.011
485 Liu Q, Zhang Q, Yan Y, Zhang X, Niu J, Svenning Jens-Christian. (2020) Ecological restoration is the
486 dominant driver of the recent reversal of desertification in the Mu Us Desert (China), Journal of
487 Cleaner Production, Doi: 10.1016/j.jclepro.2020.122241.
488 Liu, J., Li, S., Ouyang, Z., Tam, C., & Chen, X. (2008) Ecological and socioeconomic effects of China's
489 policies for ecosystem services. Proceedings of the National Academy of Sciences of the United
490 States of America, 105(28):9477-9482. DOI:10.1073/pnas.0706436105.
491 Lu, M. (2001). Vector autoregression (VAR)- an approach to dynamic analysis of geographic processes.
492 Geografiska Annaler Series B-human Geography, 83(2):67-78. DOI:10.2307/491057.
493 Mcmillin, W. D. (1991). The Velocity of M1 in the 1980s: Evidence from a Multivariate Time Series
494 Model. Southern Economic Journal, 634-648. Doi.org/10.2307/1059778.
495 Meng, J., Xiang, Y., Yan, Q., Mao, X., & Zhu, L. (2015) Assessment and management of ecological risk
496 in an agricultural–pastoral ecotone: case study of Ordos, Inner Mongolia, China. Natural Hazards,
497 79(1):195-213. DOI:10.1007/s11069-015-1836-1.
498 Quiggin, J. (2001). Environmental economics and the Murray–Darling river system. Australian Journal
499 of Agricultural and Resource Economics, 45(1), 67-94. DOI:10.1111/1467-8489.00134.

Reynolds, J. F., Smith, D. M. S., Lambin, E. F., Turner, B. L., Mortimore, M., Batterbury, S. P. J., et al. (2007) Global Desertification: Building a Science for Dryland Development. Science, 316(5826), 847–851. DOI:10.1126/science.1131634.

Runnstrom, M. (2003). Rangeland development of the Mu Us Sandy Land in semiarid China: an analysis using Landsat and NOAA remote sensing data. Land Degradation & Development, 14(2), 189-202.

Sims, C. A. (1980). Macroeconomics and reality. Econometrica. 48 (1):1–48. DOI:10.1002/ldr.545.

Wu, B., & Ci, L. (1999). Developing stages and causes of desertification in the Mu Us Sand land. Science Bulletin, 44(9), 845-849. DOI:10.1007/BF02885034.

Wu, B., & Ci, L. J. (2002). Landscape change and desertification development in the Mu Us Sandland, Northern China. Journal of Arid Environments, 50(3):429-444. DOI:10.1006/jare.2001.0847.

Wu, S., Li, J., Zhou, W., Lewis, B. J., Yu, D., Zhou, L. et al. (2018) A statistical analysis of spatiotemporal variations and determinant factors of forest carbon storage under China's Natural Forest Protection Program. Journal of Forestry Research, 29(2):415-424. https://doi.org/10.1007/s11676-017-0462-z.

Wu, Z., Wu, J., He, B., Liu, J., Wang, Q., Zhang, H., & Liu, Y. (2014) Drought Offset Ecological Restoration Program-Induced Increase in Vegetation Activity in the Beijing-Tianjin Sand Source Region, China. Environmental Science & Technology, 48(20):12108-12117. DOI:10.1021/es502408n.

Xiyan, M. (2012). A Multi-level Analysis of the Driving Forces of Land Use Changes in Mu-Us Desert in Recent 30 Years: Case Study of Uxin Banner, Inner Mongolia. Journal of Basic Science and Engineering. 20 (9):54-66 (in Chinese). DOI:10.3969/j.issn.1005-0930.2012.s1.006.

Xueying H , Guang Y , Fucang Q , et al. (2019). Spatial and Temporal Dynamic Patterns of Sandy Land in Mu Us in the Last 30 Years. Research of soil and water conservation, 26(5):144-150, 157 (in

522 Chinese).
523 Yin, R., & Yin, G. (2010) China's Primary Programs of Terrestrial Ecosystem Restoration: Initiation,
524 Implementation, and Challenges. Environmental Management 45(3): 429-441.
525 DOI:10.1007/s00267-009-9373-x
526 Ying Zhang, Lei Dong, Qian Xia et al. (2020) Effects of revegetation on climate in the Mu Us Sandy
527 Land of China. Science of the total environment, 139958. Doi.org/10.1016/j.scitotenv.2020.139958.
528 Yulin Municipal People's Government. (2020).
529 http://www.yl.gov.cn/info/iList.jsp?cat_id=10009&tm_id=147&info_id=63924
530 Yurui, L., Yansui, L., Hualou, L., & Jieyong, W. (2013). Local Responses to Macro Development Policies
531 and Their Effects on Rural System in China's Mountainous Regions: The Case of Shuanghe Village
532 in Sichuan Province. Journal of Mountain Science, 10(4), 588-608. DOI:10.1007/s11629-013-2544-
533 5.
534 Zhang, G., Dong, J., Xiao, X., Hu, Z., & Sheldon, S. (2012) Effectiveness of ecological restoration
535 projects in Horqin Sandy Land, China based on SPOT-VGT NDVI data. Ecological Engineering,
536 38(1), 20-29. DOI:10.1016/j.ecoleng.2011.09.005.
537 Zhang, L., Yue, L., & Xia, B. (2003) The study of land desertification in transitional zones between the
538 MU US Desert and the Loess Plateau using RS and GIS—a case study of the Yulin region.
539 Environmental Earth Sciences, 44(5):530-534. DOI:10.1007/s00254-003-0788-z.
540 Zhu Z D, Liu S, Yang Y L. (1984) Discussion on the possibility and reality of desertification in the cross
541 area of the farming and animal husbandry in northern China. Geographical Science (3):3-12,100.(in
542 Chinese) DOI:CNKI:SUN:DLKX.0.1984-03-000.

Figures

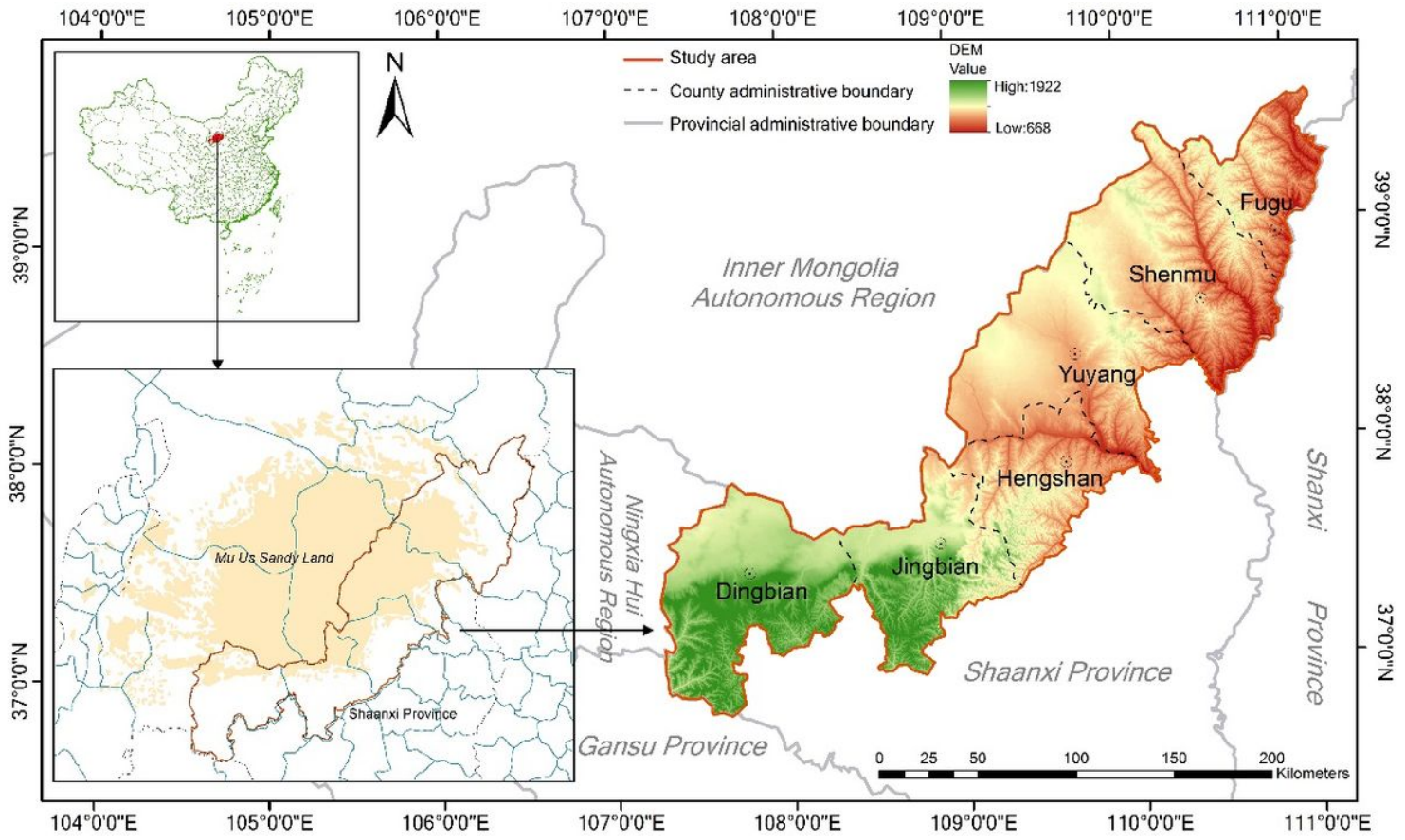

Figure 1

Location of the study area Note: The designations employed and the presentation of the material on this map do not imply the expression of any opinion whatsoever on the part of Research Square concerning the legal status of any country, territory, city or area or of its authorities, or concerning the delimitation of its frontiers or boundaries. This map has been provided by the authors.

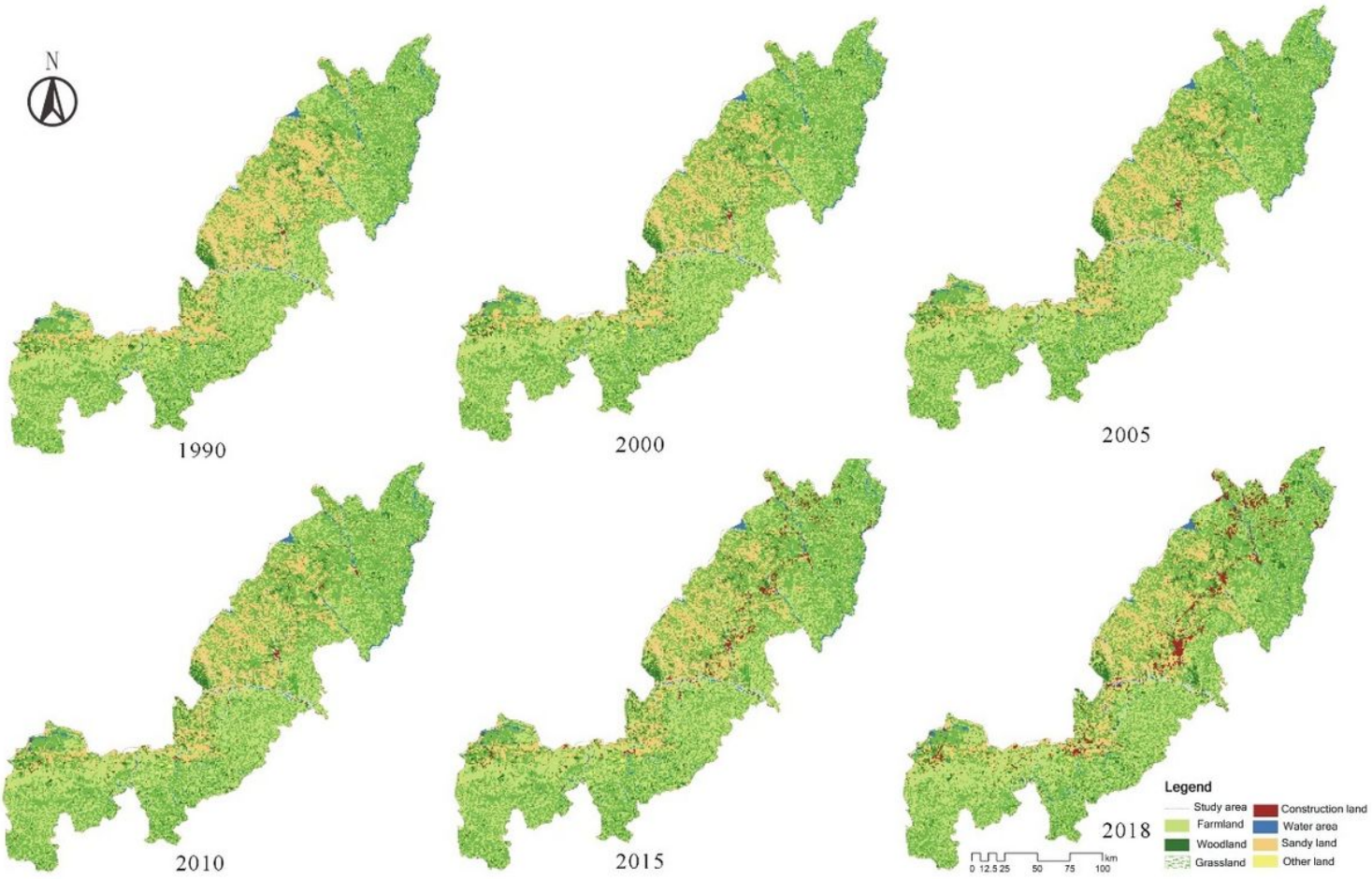

Figure 2

Land use maps of the study area from 1990 to 2018 Note: The designations employed and the presentation of the material on this map do not imply the expression of any opinion whatsoever on the part of Research Square concerning the legal status of any country, territory, city or area or of its authorities, or concerning the delimitation of its frontiers or boundaries. This map has been provided by the authors.

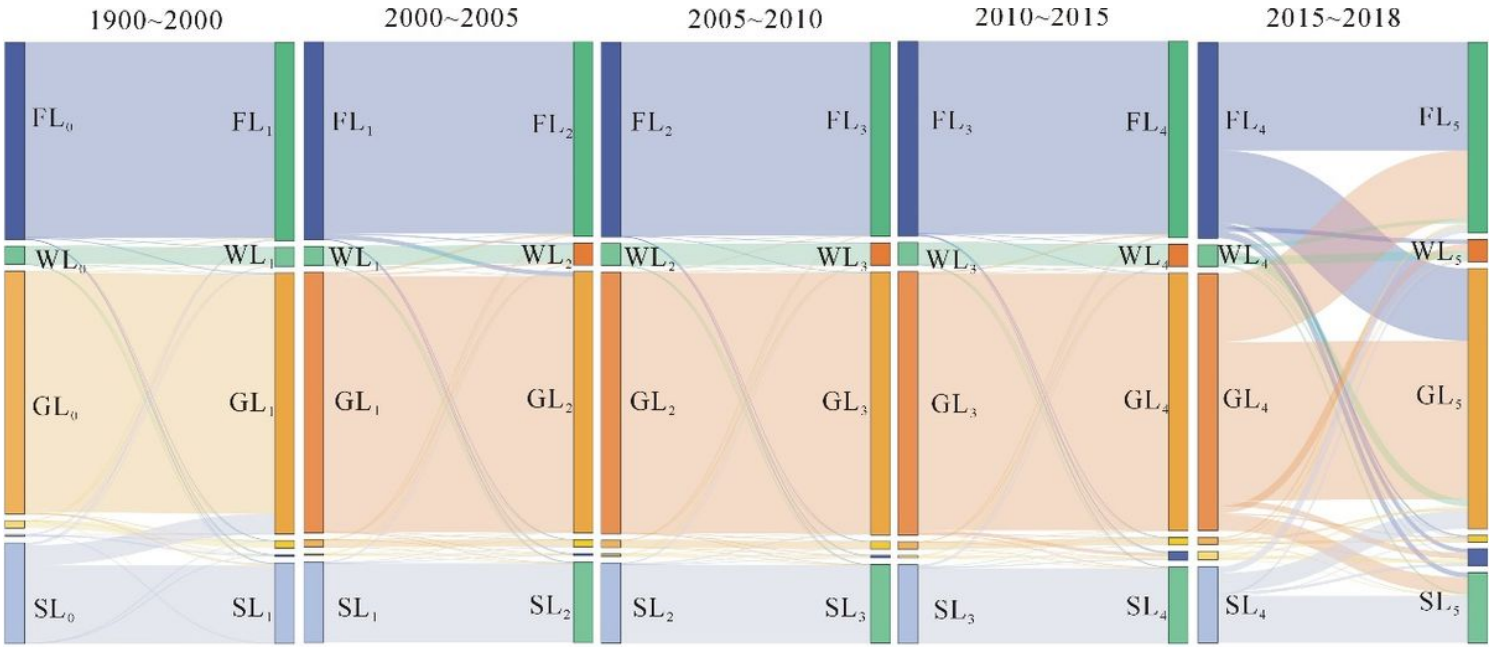

Figure 3

Sankey map of land use type conversion Note: FL denotes farmland, WL denotes woodland, GL denotes grassland, and SL denotes sandy land.

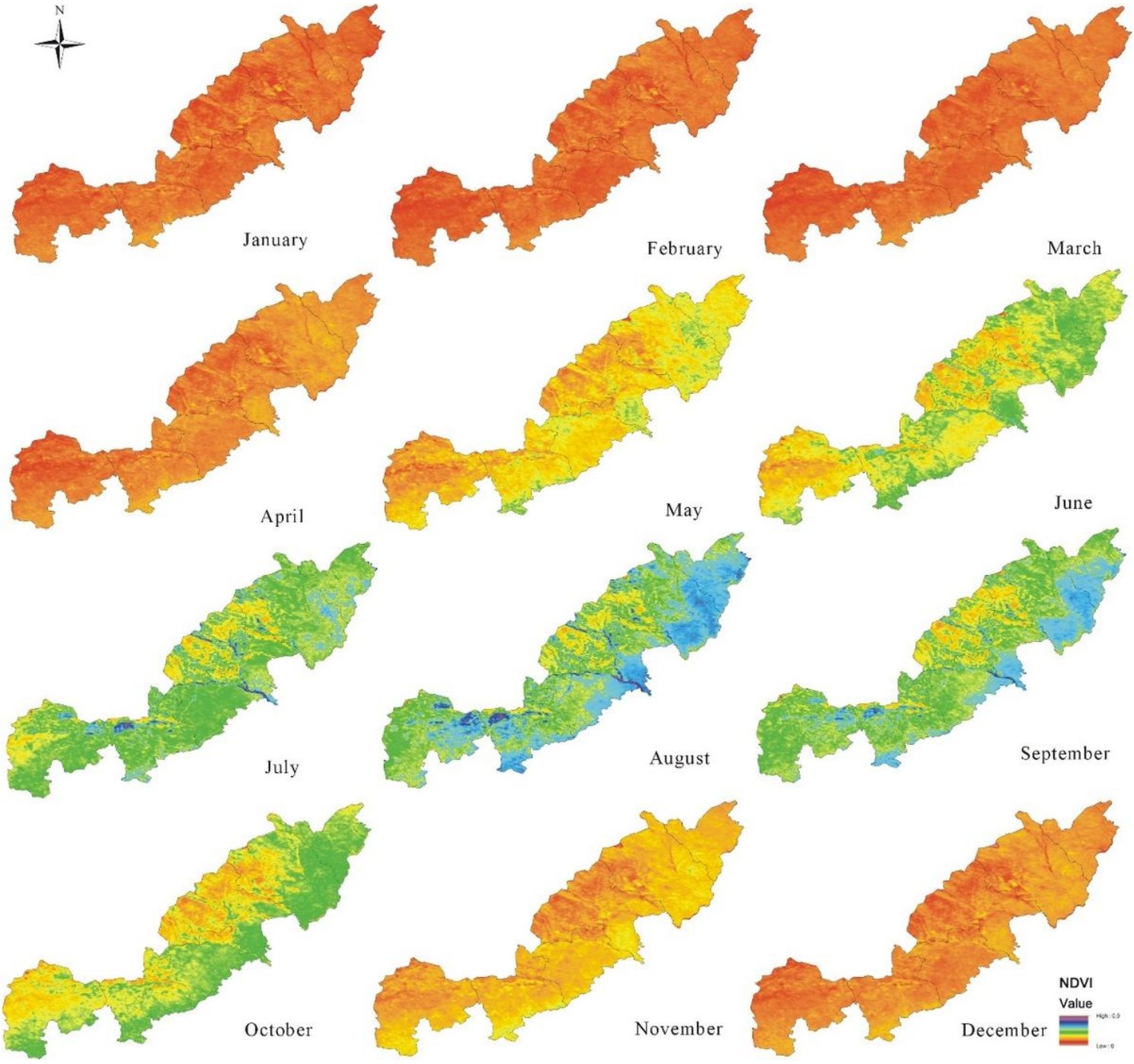

Figure 4

Distribution of the NDVI in the ANS within year Note: The designations employed and the presentation of the material on this map do not imply the expression of any opinion whatsoever on the part of Research Square concerning the legal status of any country, territory, city or area or of its authorities, or concerning the delimitation of its frontiers or boundaries. This map has been provided by the authors.

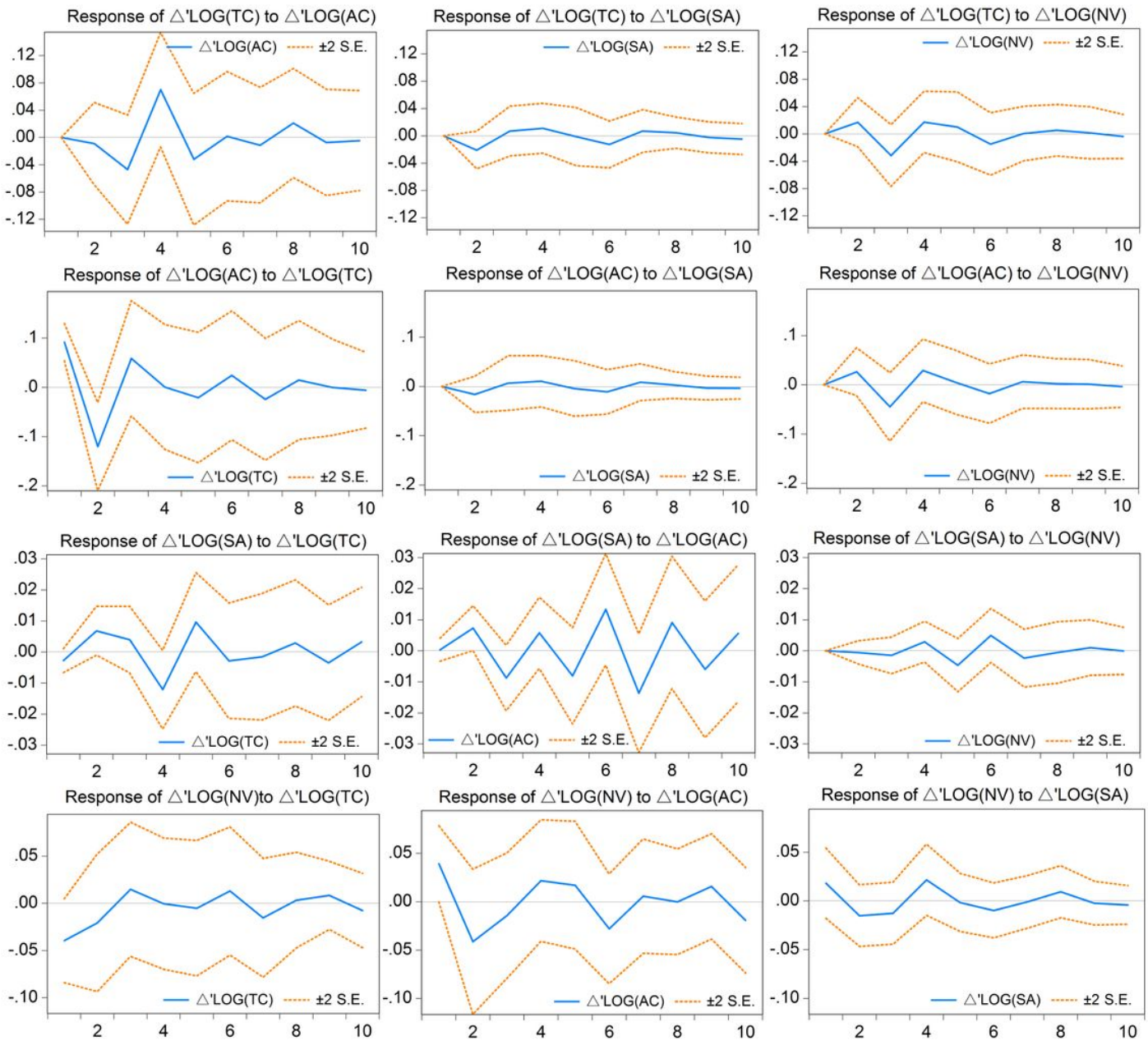

Figure 5

Impulse responses chart